Zygmunt Mikno, Szymon Kowieski, Adam Pilarczyk

Projection Welding of Nuts with Full Projections with Use of Electromechanical Operating Force System

Abstract: The projection welding of nuts performed using the pneumatic force system (PFS) was subjected to numerical and experimental analysis enabling the identification of the window of welding parameters taking into consideration boundary conditions including expulsion, torsional strength and the deformation of the nut thread. The welding process was subjected to optimisation involving the use of a new, i.e. electromechanical force system (EFS). The optimisation-related approach involved the reduction of welding current and the extension of a welding current flow time in comparison with those obtained when using the pneumatic force system. It was assumed that the acceptance criterion would be the breaking torque not lower than that obtained under the most favourable welding conditions performed using the PFS. The research work involved comparative numerical calculations (performed using the SORPAS software) in relation to both, i.e. the PFS and EFS. The technological welding tests were performed using inverter welding machines (1 kHz) provided with various (electrode) force systems. The research work also included metallographic tests and torsional strength tests. As a result of the application of EFS and a special innovative hybrid algorithm for controlling the initial electrode force, a wider and higher weld core was obtained. The depth of "penetration" into the sheet was also greater. As a result, the welded joint has a higher strength (by 30%). Technological welding tests for the new EFS system were carried out for a 25% lower welding current compared to PFS. Despite the lower welding current for EFS, the welding energy is slightly lower but the welding quality for EPS is significantly higher.

Keywords: projection welding, electromechanical operating force system

DOI: *10.17729/ebis.2019.2/1*

Introduction

Large-scale production puts demands on technologies so that they allow both rapid product and repeatable production. The automotive industry and household appliances, where the volume and complexity of products are relatively large, uses, to a large extent, resistance welding technology to connect mostly steel structures. Among the welding technologies, after the resistance spot welding, the

dr inż. Zygmunt Mikno (PhD (DSc) Eng.), mgr inż. Szymon Kowieski (MSc. Eng), mgr inż. Adam Pilarczyk (MSc. Eng) – Instytut Spawalnictwa

most-used welding technology is resistance projection welding [1]. It is used for joining both metal sheets, screw and nut elements. Two types of projections are used in resistance projection welding technology: full and embossed [2]. In this paper, the authors presented the results of welding tests for nuts with full projections.

Force is one of the three main technological parameters of the welding process. The other two parameters are the value of current and the time of current flow. The welding process is significantly influenced by the size of the contact area of the projections during welding [3], and in particular the stability of the welding current density relative to the current contact surface of the welded elements [4]. Authors [3], [5] stated that the most important parameters of the projection welding process are the production quality of the projections, their repetitiveness and the reaction of the pneumatic cylinder to reduction of the projection's height during welding.

Resistance welding devices are equipped with various types of force systems: mechanical, pneumatic, hydraulic and servomechanical. The most commonly used are devices with pneumatic pressure systems, characterized by relatively long times needed to exert the necessary pressure force. The time of applying force is from 300 ms for this type of devices. Pneumatic force system is characterised by high inertia and cannot be applied for fast force changes [6]. For this reason, the value of pre-set force is usually constant. When the force is too high, high deformation of welded elements (projections) occurs. If the force is too low, this could lead to the formation imperfections of a projection joint (high temperature in contacts, expulsion). In pneumatic systems, force applied during welding results from a specific force preset in a pneumatic cylinder. The travel of electrodes is a consequence of the action of this force and the changeable mechanical resistance of materials being welded [7].

On the other hand, a device with a servo-mechanical force system is introduced, where the travel times and the desired force are shorter and less than 100 ms [8], [9]. Using this technology very desirable lower deformation (interpenetration) of projections can be obtained and more energy can be produced in the contact area of welded elements. This new solution consists in electrode travel control, which significantly changes the previous approach to the resistance welding process (especially to projection welding of nuts) and significantly affects the development of the entire research area (pressure welding).

FEM Calculations

The research-related FEM calculations were conducted using the software SORPAS® 3D version 4.83 [10]. The software application enables carrying out associated analyses, including coupled electro-thermo-mechanical analyses. This software features a module including the effect of a new force solution and a precise electrode movement solution, i.e. by the servomechanical system. Projection welded joint is characterised by a thin layer of melted material being welded. The weld is being formed at temperature lower than the melting point. This results from the specificity of the process, i.e. material melting and squeezing of plasticised material outside a weld as a result of electrode force action.

Calculation Model

In calculations and experimental tests steel M10x22x10 nuts (Fig. 1) and 2.5 mm thick steels sheets were used. Dimensions of nut from Fig. 1 are given in table 1. For better demonstration and exact analysis of the process while performing FEM calculations, the welding area has been marked with three points for temperature measurement (Fig. 2).

The 3D model was composed of 4 379 8-node hexahedral and 6-node prismatic elements. Mentioned above elements provide three degrees of freedom (DOF) in each node for the

velocity components of plastic flow in the mechanical model and one DOF for modelling the scalar fields of temperature and one DOF for electrical potential. The solution was performed using explicit time integration scheme [11]. Lists the parameters used in the FEM calculations are given in table 2.

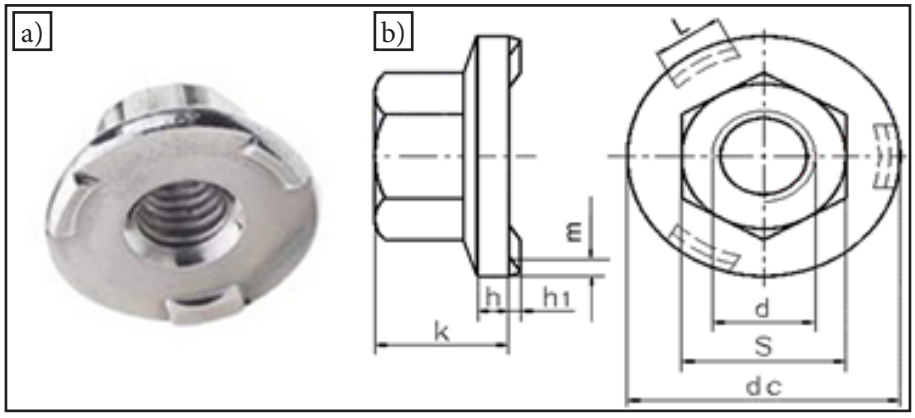

Fig. 1. Nut used in research and modeling. Nut with three full projections: a) view of the nut; b) a sketch with the dimensions indicated in the table 1

Table 1. Dimensions of the nut according to the markings from Fig. 1

***d*, mm**	***dc*, mm**	***h*, mm**
6	18	2
h_1, mm	***k*, mm**	***S*, mm**
0,85	6,85	9,75

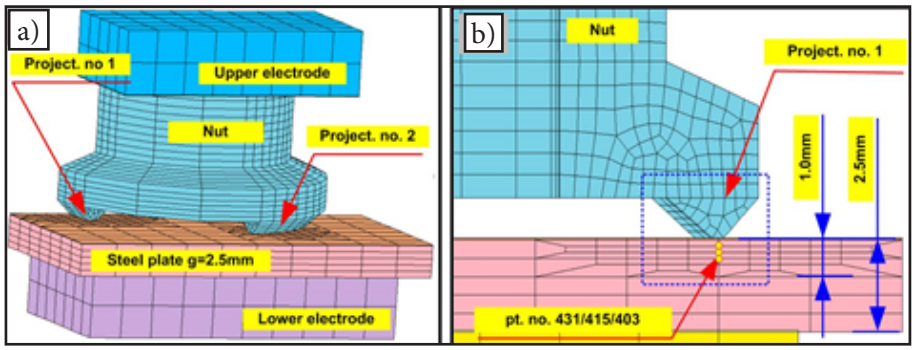

Fig. 2. FEM calculation model of the process of steels nuts resistance projection welding: a) overwiev of model, b) model with points for temperature measurement

Table 2. Parameters used in the numerical calculations

	Initial force	**Current up-slope (increase)**	**Current flow time**	**Final force**	
Pneumatic force system (PFS)	500	10-70	200	500	ms
Electromechanical force system (EFS)	200	10	250-300	500	ms
Increment	1	0.2	0.2	1	ms
Data recorded at	2	2	1	2	step
Convergence of calculations					
	Accuracy of calculations				
Electric model	1.00E-5				
Thermal model	1.00E-5				
Mechanical model	1.00E-5				
Heat emission (losses) to the environment					
Ambient (air) temperature	20			°C	
Heat transfer coefficient	300			$W/m^{2*}K$	
Other parameters					
Electrode dimensions (diameter)	30			mm	
Electrode height	10			mm	
Type of welding current	DC (1kHz)				
Type of contact between welded elements	Sliding				

Process Parameters

Based on the present recommendations and guidelines concerning the projection welding of nuts, the following range of welding parameters was adopted in relation to:

I) PFS [12][13][14]:
- i) current I=16.0÷20.0 kA, ii) current flow time tweld=10 ms (up-slope) + 200÷300 ms (primary welding time),
- ii) electrode force F=5.0÷9.0 kN,

II) EFS:
- i) current I=14.0 kA,
- ii) current flow time tweld=10 ms (up-slope) + 200÷300 ms ii) electrode displacement control during the flow of current.

For comparative purposes, also a current of 14.0 kA was subjected to analysis (in relation to the PFS). However, the above named current was overly low and precluded the making of a proper welded joint. In total, 15 variants, i.e. 12 in relation to the PFS (P1÷P12) and 3 in relation to EFS (E1÷E3) were subjected to analysis. The analysed variants along with preset welding parameters and the torsional moment obtained in destructive tests (MB) are presented in Table 3. The FEM calculations involved the adoption of material data from the (Sorpas) software [10]:

1. nut – AISI 1017IW.Nr.1.0037 (Hr): CO.20 Mn0.6, solidus - 1500°C, liquidus - 1510°C,
2. sheet – HSLA 420 SAE J 2340 420X – 420LAD, solidus - 1500°C, liquidus - 1510°C,
3. electrode – grade A3-1.

Experimental tests

The technological welding tests involved the making of a nut-sheet welded joint, frequently used when joining car body elements. Nut M10x22x10 (SAE 1015) with three symmetrically arranged projections (total base of projections amounted to 65 mm^2) was welded to 2.5 mm thick sheet made of DKP-S550MC-O (PN-EN 10149-2) (without protective coating), 300 mm x 3000 mm, at 50 mm intervals. Before welding, the sheet was degreased. The chemical compositions of the welded materials (nut and sheet) are presented in Tables 7 and 8 respectively. The technological welding tests were performed using an inverter welding machine (1 kHz), the PFS (Fig. 3a) and EFS (Fig. 3b).

Table 3. Analysed variants in the numerical model and technological welding tests

No.	Variant	Electrode force system	Welding parameters				Remarks
			Current	Time	Force		
			kA	ms	kN		
1	P1	Pneumatic (PFS)	14.0	200	5.0		M_B < 50 Nm
2	P2				7.0		
3	P3				9.0		
4	P4		16.0		5.0		M_B < 200 Nm
5	P5				7.0		M_B < 150 Nm
6	P6				9.0		M_B < 50 Nm
7	P7		18.0		5.0		*OK*, M_B < 220 Nm
8	P8				7.0		M_B < 200 Nm
9	P9				9.0		M_B < 150 Nm
10	P10		20.0		5.0		thread deformation, expulsion
11	P11				7.0		*OK*, M_B < 220 Nm
12	P12				9.0		thread deformation
13	E1	Electro mechanical (EFS)	14.0	250	forging	6.0	*OK*, M_B < 230 Nm
14	E2			300		6.0	*OK*, M_B < 270 Nm
15	E3			300		9.0	*OK*, M_B < 300 Nm

Table 4. Chemical composition of nut M10x22x10 (SAE 1015, wt. %)

C	Mn	P	S	Fe
0.17	0.44	0.013	0.008	Bal.

Table 5. Chemical composition of sheet DKP-S550MC-O (1434, wt %)

C	Mn	P	S	Si
0.065	0.91	0.008	0.007	0.014
Al	**Nb**	**V**	**Ti**	**Fe**
0.032	0.063	0.003	0.039	Bal.

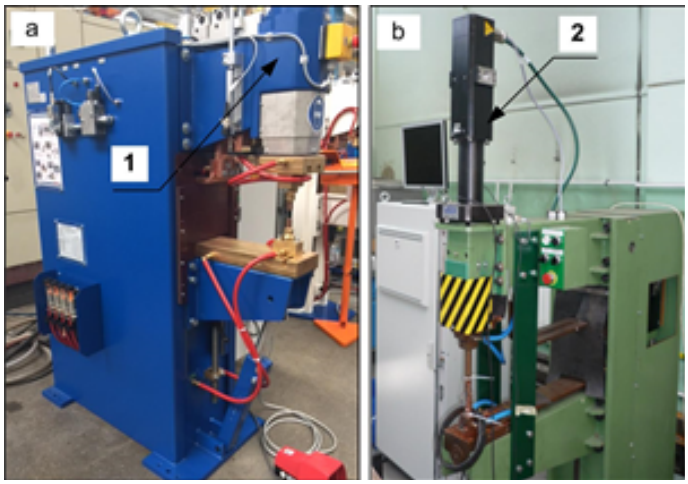

Fig. 3. Test rig for technological welding tests provided with: a) PFS, b) EFS, 1) pneumatic actuator, 2) servomotor

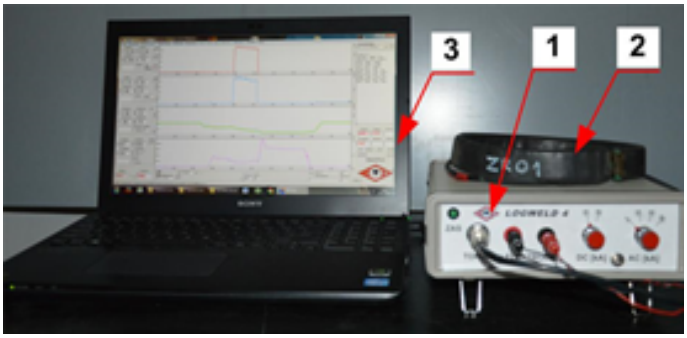

Fig. 4. LogWeld-4 device for measurements of characteristic parameters of the resistance welding process, 1) measurement interface, 2) Rogowski coil, 3) PC

The results obtained in numerical calculations were verified experimentally in technological welding tests, metallographic tests, and torsion tests as well as through measurements of selected characteristic parameters of the welding process including welding current and voltage, displacement of electrodes (projection height reduction) and electrode force. Characteristic parameters were recorded using a LogWeld 4 measuring device (Fig. 4). The functions of the measuring device also enabled the performance of the analysis of (current and voltage) derivative parameters, e.g. waveform of static slope resistance, momentary power and energy supplied to the welding area. The above-named parameters referred to the entire welding area. The device also featured the analysis of waveforms, i.e. reading of momentary values and recorded variable values in relation to a time span marked using the cursor.

The specimens used in the metallographic tests were subjected to chemical etching using Nital.

The parameters preset in relation to the PFS (grey) and two most favourable variants are presented in Table 6 (P7, P11). The remainder of

Table 6. Preset parameters and characteristic parameters in relation to the PFS

No.	Variant no.	Preset parameters							Recorded parameters					
		Force	Up-slope		Main welding time		Total current (I_{rms})	Main interval current (I_{rms})	Energy	Projection height reduction	Weld width	Weld height	Breaking torsional moment (M_B)	Number of specimens
			Current	Time	Current	Time								
		kN	kA	ms	kA	ms	kA	kA	kJ	mm	mm	mm	Nm	pcs
		A	B1	B2	C1	C2	D1	D2	E	F	G	H	I	J
1	P7	5.0	18.0	50	18.0	150	17.8	18.0	8.3	0.74	2.1	0.05	220	30
2	P11	7.0	20.0	50	20.0	150	19.7	20.0	9.5	0.95	2.1	0.06	220	30
Key: I rms – root-mean-square current														

Table 6 presents characteristic parameters describing the welding process. These parameters included energy supplied to the welding area, a breaking torque (MB) as well as the width and depth of the weld. Unfavourable effects such as expulsion, nut thread deformation or the overheating on the other side of the sheet were not observed in relation to the above-named parameters. In both cases the mean value of the breaking torque in the torsion test amounted to 220 Nm.

Process optimisation

Optimization of the projection welding process using an electromechanical pressure system was carried out experimentally. Optimization included applying a reduced welding force at the beginning of the welding process and controlling the movement of the electrodes during the welding current flow. The presented conditions enable more favourable heat generation at the point of contact between the projection of nuts and sheet metal. This location of the heat causes a more intense melting of the welded materials. The parameters preset in relation to the EFS (grey) and three most favourable variants are presented in Table 7.

In comparison to PFS technology, a reduced current value (14 kA) was used. Despite reduced current experimental welding parameters allowed for higher torsional strengths comparing to PFS, where the breaking torque was less than 50 Nm. The experiments included modification of the following parameters: time of welding current flow, initial and upsetting welding force and displacement of electrodes (table 7, exemplary variants E1÷E3). In table summary time and displacement of electrodes are given.

Results of optimisation of the process

The results of welding tests with PFS were transferred to the FEM model using the parameters used in the experiments. The results of the modelling were analysed in terms of the size (Fig. 5a, c) and volume (Fig. 5g) of the weld nugget, depth of penetration in the metal sheet (Fig. 5e) the displacement of the electrodes at the end of the welding current flow(Fig. 5b) the

Table 7. Preset parameters and characteristic parameters in relation to the EFS

No.1	Variant no.	Preset parameters											Recorded parameters					
		Force			Up-slope		Main welding time		Total current (I_{rms})	Main interval current (I_{rms})	Summary time and displacement of electrodes	Upsetting force	Energy	Projection height reduction	Weld width	Weld height	Breaking torsional moment (M_B)	Number of specimens
		Initial	Minimum	Maximum	Current	Time	Current	Time			t/Δl							
		kN			kA	ms	kA	ms	kA	kA	ms/mm	kN	kJ	mm	mm	mm	mm	pcs
		A1	A2	A3	B1	B2	C1	C2	D1	D2	E	F	G	H	I	J	K	L
1	E1	3.5	2.5	6.3	14.0	10	14.0	240	14.1	14.4	250 0.55	6.0	6.7	0.71	2.9	0.50	230	30
2	E2	---	---	---	---	---	---	290	---	---	300 0.60	6.0	7.5	0.75	3.0	0.53	270	30
3	E3	---	---	---	---	---	---	---	---	---	---	9.0	7.5	0.9	3.1	0.55	300	30
Key: I_{rms} – root-mean-square current , „ ---„ – value identical as in the line above																		

displacement of the electrodes at the end of the entire process (Fig. 5d) and the energy supplied to the weld(Fig. 5f). On Fig. 6 results of experiments with use of the PFS are presented in the form of joints quality dependence from weld current and force. The green colour on Fig. 6 of ribbon-shaped area indicates the correct welding quality characterized by torsional strength higher than 200 Nm.

On the above-mentioned drawing, areas of insufficient torsional strength of weldment (blue and red) were also marked. The dashed line shows the area of parameter sets at which the thread deformation and/or the expulsion occurred. The designation P1÷P12 responds to welding parameters described in table 3.

The results of the experiments were compared with the results of modelling (Fig. 7). The use of PFS technology makes it possible to obtain a relatively small welding nugget – melted area (Fig. 7a1). In contrast, the use of optimized EFS technology allows a much larger melted

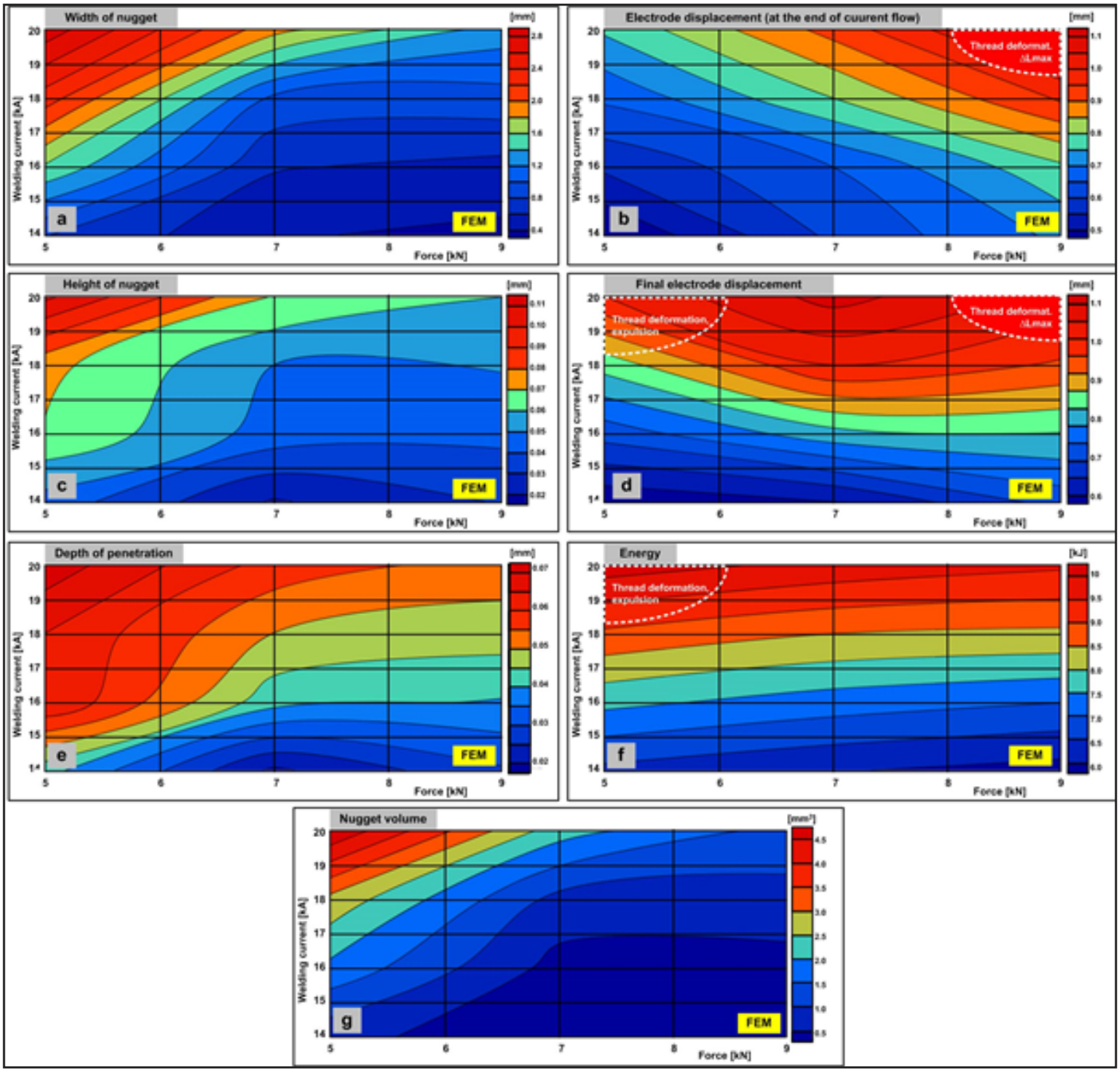

Fig. 5. The results of optimisation FEM model calculations for PFS: a) width of nugget, b) the displacement of the electrodes at the end of the welding current flow, c) height of nugget , d) the displacement of the electrodes at the end of the entire process, e) depth of nugget penetration in the metal sheet , f) energy supplied to the welding area, g) volume of the weld nugget

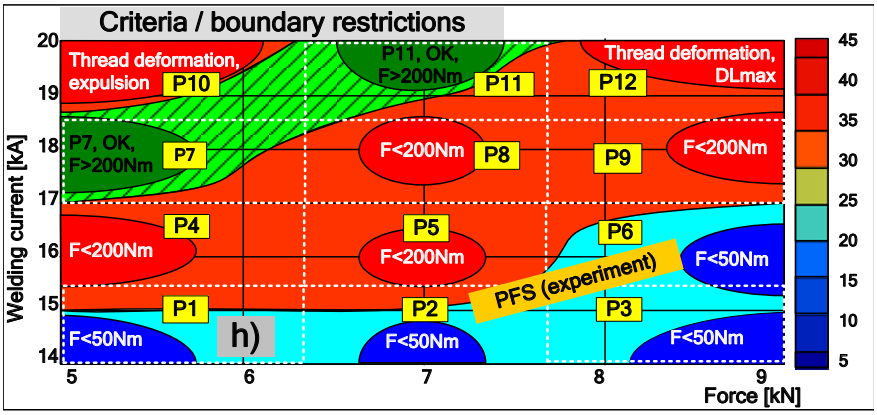

Fig. 6. The results of experiments for PFS – results of joint quality obtained in experiments.

area of the connected elements (Fig. 7b1). The test results of welded joints as well as the results of modelling (Fig. 7a1 and 7b2) converge and confirm the validity of using the proposed welding program.

The results of the experiments were compared with the results of modelling at three points located below the faying surface under the projection in the sheet (Fig. 2 b, Fig. 8). The results of microscopic examination and modeling results for both PFS and EFS systems were compared.

The use of PFS technology makes it possible to obtain a relatively small area of melting, which resulted in the points D, E and F being located outside the area of the weld core (Fig. 8 c). Modelling results revealed that the maximum values (Fig. 8d) are lower than the melting temperature of steel and are respectively 1383°C, 1340°C and 1284°C. In contrast, the use of the optimized EFS technology allows a much larger area of melting of the joined elements, which was shown on the results of microscopic tests (Fig. 8a). Modelling results in the form of temperature waveforms for points (A, B, C from Fig. 8) placed in the same grid locations as for PFS technology reach temperatures above the melting point. The temperature at these points reaches 1590°C, 1562°C and 1525°C respectively. For the PFS system, the welding area has dimensions 58x830 µm, while for the EFS system this area is larger 567x2976 µm. Both technologies were implemented using a similar amount of energy.

Conclusions

The direction of changes resulting from the use of the EFS and the algorithm of electrode force and displacement control entirely different from previously adopted approaches. Undertaken activities produced a positive and very desirable effect in the form of more favourable space distribution of welding power, i.e. increased welding power density, particularly in the contact area between elements being welded.

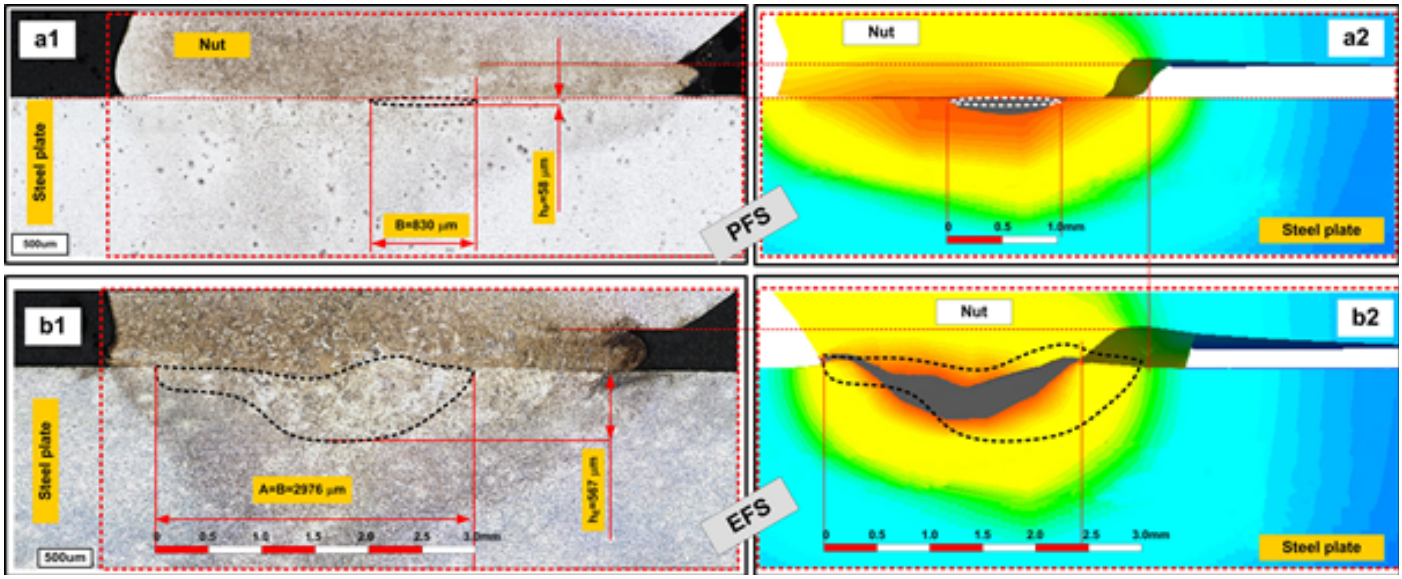

Fig. 7. Results of the experiments and results of modelling with use of PFS and EFS technology.

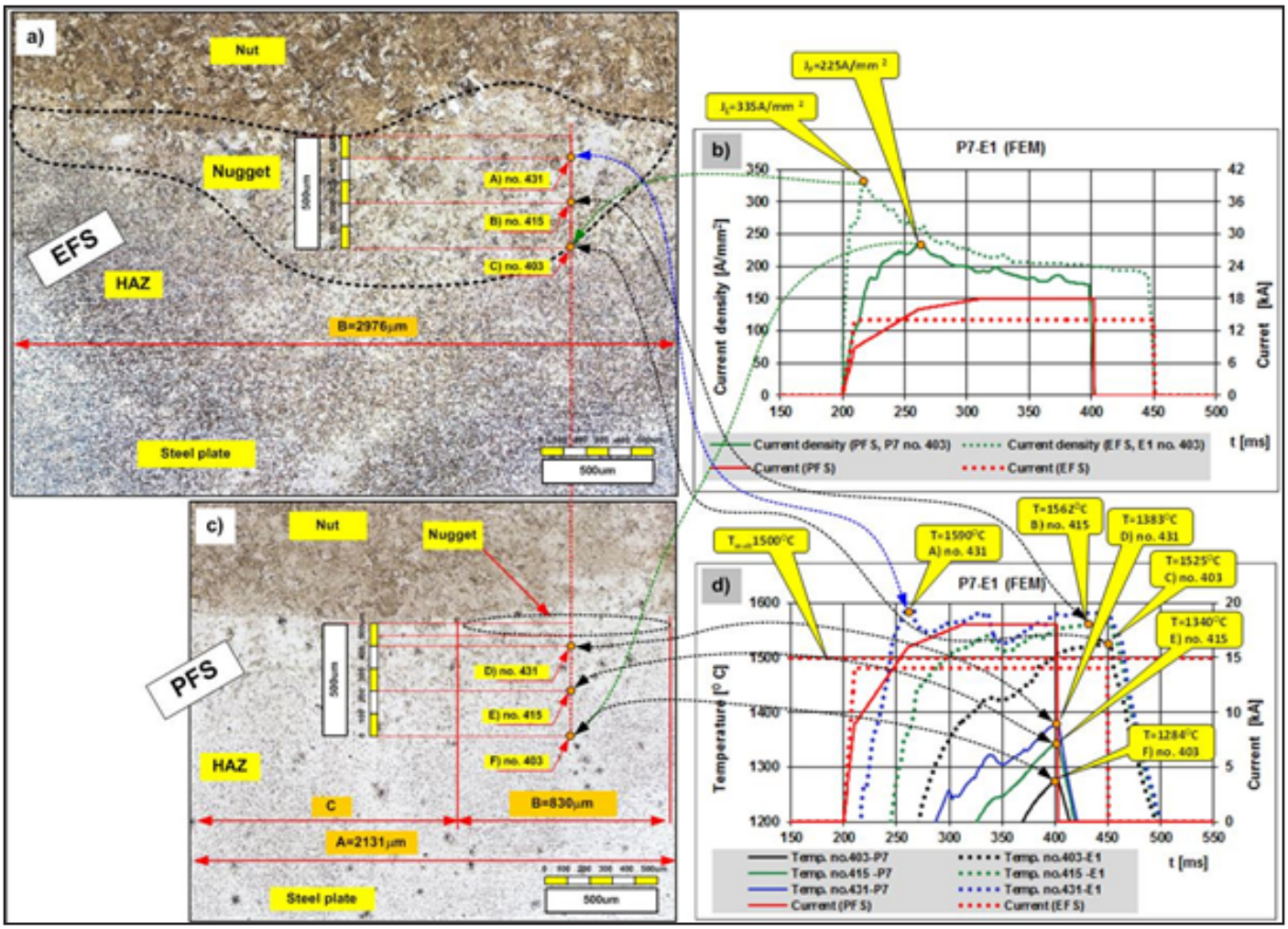

Fig. 8. Results of the experiments and results of modelling computations for determining the current density (b) and temperature waveforms (d) for points form (Fig. 2b). Results of modelling results are compared with the results of experiments for both PFS (c) and EFS (a) technology

The welding process performed using the EFS involved the use of a lower welding current of 14.0 kA (by 28%) than that used during welding performed using the PFS (18.0 kA). In spite of the foregoing i) volume of the weld nugget molten material increased more than 4 times , ii) penetration depth increased (exp. 10 times from 58 µm to 567 µm), iii) welding energy was slightly lower (exp. from 4.6 kJ to 4.4 kJ), iv) breaking torque (MB) increased by 30% (exp. from 220 Nm to 300 Nm).

Acknowledgments

This work was supported by the Polish National Centre for Research and Development (TANGO1/267374/NCBR/2015).

References

[1] Larsson J., 2008, Projection welding for nut and bolt attachment, The Fabricator.

[2] J. S. Agapiou, T. A. Perry, 2013. Resistance mash welding for joining of copper conductors for electric motors. Journal of Manufacturing Processes, Volume 15, Issue 4, October, pp. 549–557.

[3] Sun B., 2001, Effect of Projection Height on Projection Collapse and Nugget Formation - A Finite Element Study, Supplement To The Welding Journal.

[4] Mikno Z., Ambroziak A, Senkara J., Bartnik Z., Korzeniowski M. Kowieski Sz., Węglowski M., Pilarczyk A., 2011-2013, Numeryczne i eksperymentalne badania porównawcze zgrzewania garbowego z zastosowaniem pneumatycznego i serwomechanicznego docisku elektrod,

raport z projektu badawczego N N501 196940, realizacja 2011-2013, kierownik projektu – Zygmunt Mikno.
[5] J. Gould. Joining Aluminium Sheet in the Automotive Industry-A 30 Year History. 2012. Welding Journal (Welidng Res.) vol91. January,pp.23-34
[6] www.weldtechcorp.com
[7] Z. Mikno. 2016. Projection Welding with Pneumatic and Servomechanical Electrode Operating Force Systems. Welding Journal (Welidng Research) 2016 vol 95. August, pp. 1-13.
[8] S. A. Slavick. 1999.Using Serwoguns for Automated Resistance Welding, Welding Journal vol. 78, no7.
[9] Zhang H., Senkara J., 2011, Resitance welding Fundamentals and Applications, Taylor&Francis Group.
[10] Swantec Inc. SORPAS Software model 3D Version 4.0 x 64 http://swantec.com/
[11] Nielsen C.V., Zhang W., Alves L.M. Bay N., Martins P.A.F., 2013, Modelling of Thermo-Electro-Mechanical Manufacturing Processes - Applications in Metal Forming and Resistance Welding, Springer Briefs in Applied Sciences and Technology.
[12] H. Papkala. Zgrzewanie oporowe metali. Wydawnictwo KaBe Krosno 2003.
[13] AWS Welding Handbook 9th edition , volume 3, welding processes, part 2 chapter 2, projection welding.
[14] Gould JE (1993) Projection Welding. ASM International, ASM Handbook. Vol. 6: Welding, Brazing, and Soldering (USA), pp. 230-237, 1993.